Bifurcation Elimination in Rotor Gas Bearing Systems Applying Numerical Continuation with Embedded Design Optimization Scheme

Panagiotis Papafragkos, Ioannis Gavalas, Ioannis Raptopoulos and Athanasios Chasalevris
School of Mechanical Engineering, National Technical University of Athens, Athens, Greece

Abstract

High speed rotor systems mounted on gas foil bearings present bifurcations which change the quality of stability, and may compromise the operability of rotating systems, or increase noise level when response amplitude drastically increases. The paper identifies the dissipating work in the gas film to be the source of self-excited motions driving the rotor whirling close to bearing's surface. The energy flow among the components of the system is evaluated for various design sets of bump foil properties, rotor stiffness and unbalance magnitude. The paper presents a methodology to retain the dissipating work at positive values during the periodic limit cycle motions caused by unbalance. An optimization technique is embedded in the pseudo arc length continuation of limit cycles, those evaluated (when exist) utilizing an orthogonal collocation method. The optimization scheme considers the bump foil stiffness and damping as the variables for which bifurcations do not appear in a certain speed range. It is found that Neimark-Sacker bifurcations, which trigger large limit cycle motions, do not exist in the unbalanced rotors when bump foil properties follow the optimization pattern. Period doubling bifurcations are possible to occur, without driving the rotor in high response amplitude. Different design sets of rotor stiffness and unbalance magnitude are investigated for the efficiency of the method to eliminate bifurcations. The quality of the optimization pattern allows optimization in real time, and bearing properties shift values during operation, eliminating bifurcations and allowing operation in higher speed margins.

Introduction

Gas Foil Bearings (GFBs) are part of a promising oil-free technology in modern high-speed rotating machinery, distinguished for their reliability, simplicity, and environmentally friendly characteristics. Relying on a thin gas film building up an aerodynamic, load-carrying lubrication wedge, such bearings are self-acting and do not require any external pressurization. Most notably, due to the absence of solid-to-solid contact between the airborne rotor journal and the bearing sleeve, excessively low wear and power loss can be achieved. Several types of GFBs have been introduced in the past, with the most common and efficient being the bump type foil bearing. The major difference detected in comparison with the conventional oil bearings is the presence of a thin gas film as a lubricant, which results to building up an aerodynamic, load-carrying lubrication wedge and eliminates the need for external pressurization [1-4].

During the last few decades, the potential of GFBs has been widely confirmed by a great number of successful applications in air cycle machines of commercial aircraft [5]. Lately, in particular as a result of insurmountable speed, temperature, and weight limitations of conventional rolling-element bearings, novel concepts of oil-free turbochargers [6], oil-free rotorcraft propulsion engines [7], and micro gas turbines [8] are gaining increasing interest. Gas foil bearings have been successfully used in high-speed turbomachines, and they present a remarkable reliability. As the stiffness of the foils is much smaller than that of the fluid film, the foil bearings can adapt to various working conditions through foil deformations. Owing to these advantages, foil bearings are identified as a potential alternative for oil bearings. If properly designed and operated, foil bearings would incur very slight wear and have a long service life [7].

The design of a GFB is a multi-physical problem, and the research work on GFBs follows generically scientific objectives which have to couple each other at most times; these are mainly a) the material development (super alloys) for use in the GFB components [3], b) the fluid-structure interaction including the aerodynamic lubrication problem (compressible flow) and the structural problem predicting the bump foil structure dynamic properties and dynamic behaviour [9-12], c) the nonlinear dynamics of simple or complex rotors mounted on GFBs [13-19], d) the development of alternative GFB configurations including also adjustable configurations and control schemes [20].

Nonlinear dynamics of rotor-GFB systems, and its study with tools like continuation methods, is relatively new object. Continuation methods have been applied on the nonlinear dynamics of rotor systems on oil bearings of several types [21,22], and recently in GFB rotor systems as well [23]. Bifurcations of Hopf type have been investigated at both bearing types (with oil and gas) [24]. The strongly nonlinear aerodynamic forces render a variety of motions and stability quality in the system, including periodic, quasi periodic and chaotic motions. Further to that, the system has the potential of totally different motions even at the same operating speed, according to initial conditions and operating parameters, such unbalance magnitude. Dynamic systems present stable and unstable solution branches and respective bifurcation sets, and this is the case in rotor-GFB systems too. Nonlinear dynamics of rotor-GFB systems were mostly used to correlate the quality of response of the system with advances in top/bump foil structure simulation, or alternative models in the aerodynamic simulation.

Further to the aerodynamic modelling and, the bump type foil modelling has been investigated during the last decades as its properties are directly correlated to the aerodynamic performance of the bearing. Heshmat et al. [1] introduced the so-called simple elastic foundation model, consisting of linear elastic uncoupled springs. No viscous damping was taken into account until Peng and Carpino [9] and Ku and Heshmat [26] took into consideration the top-to-bump foil and bump-to-housing Coulomb friction damping. Later on, Peng and Carpino [27] introduced a 2D foil model structure characterized by linear stiffness and damping coefficients, while considering the elastic behaviour of the bump foil. Alternative approaches have been published by Lez et al. [25] and other researchers [23], where the foil bumps and their interaction are modelled by multi-degree freedom systems. Baum et al. [12] introduced another foil structure, consisting of rigid, massless, beam-like elements with one finite dimension in axial direction and no coupling of the elements in the circumferential one, where each bump foil is modelled by a non-linear spring and a linear damper.

This paper aims to the insight of the local instability mechanisms, which trigger bifurcations, and drive the response of the system far from its elastic response (self-excited vibrations), usually close to the bearing clearance in journal positions and the rotor-stator clearance along the rotor. In this paper, it is found that the dissipating energy in the gas film should be directly correlated to the first (at lower speed) bifurcation detected in such a system, this being a Neimark-Sacker bifurcation in the unbalanced system, at most cases, or a period-doubling (flip) bifurcation in some others. Specifically, this paper benefits from the well-known lemma that self-excited motions are triggered when negative damping is included in the system; similar notification was made in [28] for rotors on oil bearings, under linear harmonic analysis. The energy flow is evaluated in this system for various design sets and this is used to an optimization scheme to avoid bifurcations in a certain speed range. The paper is organized as follows:
The dynamic system of consisting of an elastic Jeffcott rotor mounted on two GFBs is composed for the autonomous and the non-autonomous case. The composition of the system renders a set of ordinary differential equations of 1st order (ODE set). The aerodynamic lubrication model and the bump foil structural model follow existing literature [12,14]. The authors program the pseudo arc length continuation method [29-31] with embedded orthogonal collocation method to provide the potential periodic solutions of the ODE set with unbalance excitation.

Moreover, the quality of motions developed in such system is discussed evaluating the bifurcation sets, the time-frequency decomposition of the response and Floquet multipliers, for some design scenarios and at a certain speed range. The energy flow is evaluated in the system during the respective periodic motions, with primary interest on the dissipative work of gas forces. An optimization scheme of successive polls for the two GFB design variables is implemented from the literature [32] and retains the dissipative work in the gas film positive in the respective speed range; Neimark-Sacker bifurcations are found to be eliminated in the respective speed range. However, period doubling bifurcations still exist at some cases, without these to drive the response at high amplitudes though. Different rotor stiffness and unbalance magnitude are considered in the results. The paper concludes that maximizing the dissipative work in the gas film does not trigger self-excited motions of the system, in a certain operating speed range, approximately two times wider than the respective without optimization of the GFB properties.

Modelling and Formulation of the Nonlinear Dynamic System

The physical model of the flexible rotor and of the gas foil bearings is presented in Fig. 1 where the symmetric rotor model considers the well-known Jeffcott rotor. The analytical dynamic model includes 4 DoFs for the rotor (due to symmetry), and the unique parameter of rotor design included in the model is the rotor's lateral stiffness $\bar{k}_s$. The gas foil bearing model [2] considers linear spring and damping properties in the bump foil in the radial direction, and the key parameters of the gas bearing design consider the bump foil compliance $\bar{\alpha}_f$, and the pump foil damping coefficient c_f as a function of the loss factor η.

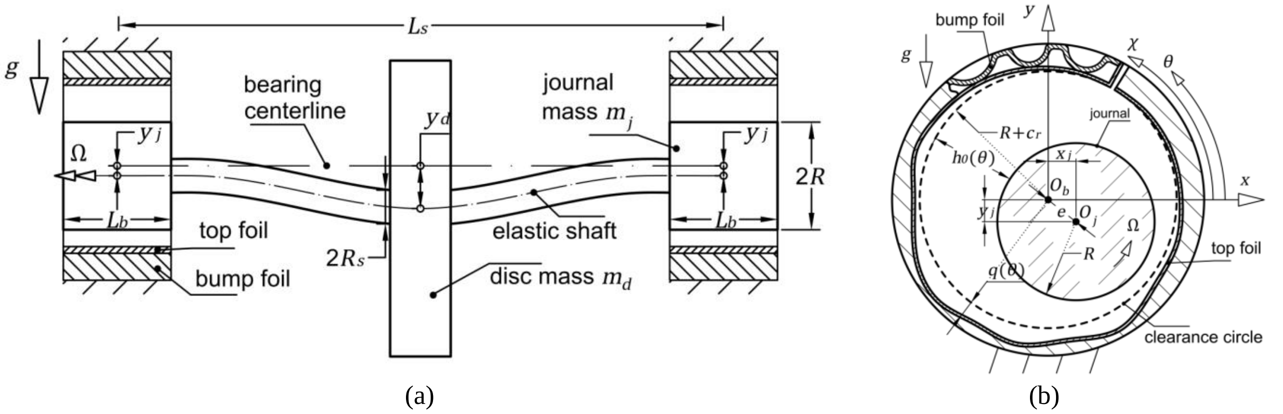

Figure 1: a) representation of an elastic Jeffcott rotor model with two journal masses at its ends, mounted on two gas-foil bearings; b) representation of the gas foil bearing configuration

Analytical model of the gas bearing

The assumptions introduced in the elastoaerodynamic lubrication problem are: a) isothermal gas film, b) laminar flow of the gas, c) no-slip boundary conditions, d) continuum flow, e) negligible fluid inertia, f) ideal isothermal gas law $\left(p/\rho = \text{constant}\right)$, g) negligible entrance and exit effects, and h) negligible curvature $\left(R \approx R + c_r\right)$. The Reynolds equation for compressible gas flow under these assumptions is given in Eq. (1) [12], and it is an implicit function of time and of journal and top foil kinematics.

$$\frac{\partial}{\partial \bar{x}}\left(\bar{p}\bar{h}^3\frac{\partial \bar{p}}{\partial \bar{x}}\right)+\kappa^2\frac{\partial}{\partial \bar{z}}\left(\bar{p}\bar{h}^3\frac{\partial \bar{p}}{\partial \bar{z}}\right)=\bar{\Omega}\frac{\partial}{\partial \bar{x}}\left(\bar{p}\bar{h}\right)+2\frac{\partial}{\partial \tau}\left(\bar{p}\bar{h}\right) \tag{1}$$

Analytical solution for Eq. (1) cannot be defined; a common approach to evaluate the pressure distribution is the FDM. The pressure domain is converted into a grid of $i=1,\ldots,N_X+1$ and $j=1,\ldots,N_Z+1$ points, where i and j are the indexes in the circumferential and axial direction respectively, see Fig. 3a.

The Reynolds equation is first rewritten defining the first time derivative of the pressure in Eq. (2a) and after some math in Eq. (2b). Then, the discrete Reynolds equation is defined in the grid points expressing the partial derivatives with finite differences.

$$\frac{\partial}{\partial \tau}\left(\bar{p}\bar{h}\right)=\frac{1}{2}\frac{\partial}{\partial \bar{x}}\left(\bar{p}\bar{h}^3\frac{\partial \bar{p}}{\partial \bar{x}}\right)+\frac{\kappa^2}{2}\frac{\partial}{\partial \bar{z}}\left(\bar{p}\bar{h}^3\frac{\partial \bar{p}}{\partial \bar{z}}\right)-\frac{\bar{\Omega}}{2}\frac{\partial}{\partial \bar{x}}\left(\bar{p}\bar{h}\right) \tag{2a}$$

$$\dot{\bar{p}}=\frac{1}{2\bar{h}}\frac{\partial}{\partial \bar{x}}\left(\bar{p}\bar{h}^3\frac{\partial \bar{p}}{\partial \bar{x}}\right)+\frac{\kappa^2}{2\bar{h}}\frac{\partial}{\partial \bar{z}}\left(\bar{p}\bar{h}^3\frac{\partial \bar{p}}{\partial \bar{z}}\right)-\frac{\bar{\Omega}}{2\bar{h}}\frac{\partial}{\partial \bar{x}}\left(\bar{p}\bar{h}\right)-\frac{\bar{p}\dot{\bar{h}}}{\bar{h}} \tag{2b}$$

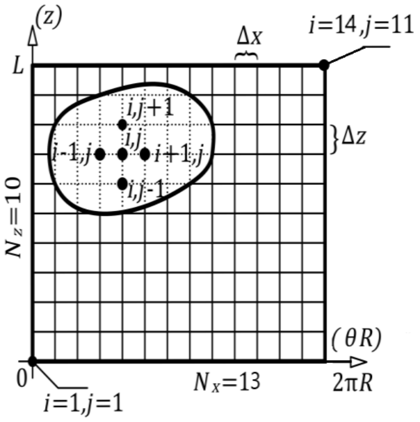

Figure 2a: Finite difference grid $N_x \times N_z$ used for the evaluation of pressure distribution

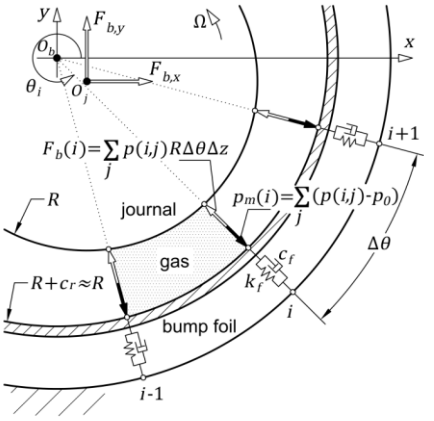

Figure 2b: Definition of the mean pressure p_m applied over bearing length L_b, and of gas force F_b with respective indexes.

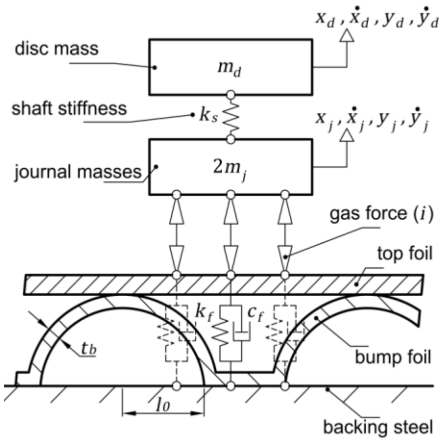

Figure 2c: Representation of the physical model; bump foil is modelled by linear springs and dampers.

The dimensionless parameters of gas pressure $\bar{p}$, gas film thickness $\bar{h}$, spatial coordinates (circumferential and axial respectively) θ and $\bar{z}$, time τ, rotating speed $\bar{\Omega}$, and ratio $\kappa = R/L_b$ are included in the elastoaerodynamic lubrication problem of Eq. (1). The gas film thickness function is defined in Eq. (3) for the continuous and the discrete pressure domain (finite difference grid) where $\bar{q}=\bar{q}(\theta)$ (or $\bar{q}_i=\bar{q}(\theta_i)$ in the discrete pressure domain) is the foil deformation in radial direction, see also Fig. 2a and Fig. 3b.

$$\bar{h}=1-\bar{x}_j\cos\theta-\bar{y}_j\sin\theta+\bar{q}, \qquad \bar{h}_i=1-\bar{x}_j\cos\theta_i-\bar{y}_j\sin\theta_i+\bar{q}_i \tag{3}$$

Boundary and initial conditions of the problem are defined in continue. Ambient pressure is assumed at the starting and ending angle of the foil (periodic boundary condition) in Eq. (4), in the continuous and the discrete pressure domain respectively.

$$\bar{p}\left(\tau,\theta_0,\bar{z}\right)=\bar{p}\left(\tau,\theta_0+2\pi,\bar{z}\right)=1, \qquad \bar{p}_{1,j}=\bar{p}_{N_X+1,j}=1 \tag{4}$$

Taking into account the symmetry of the lubrication problem, instead of assuming the gas pressure equal to the ambient p_o at the axial ends, $\bar{p}\left(\bar{z}=0\right)=\bar{p}\left(\bar{z}=1\right)=1$, the boundary condition can be written in Eq. (5) (for the continuous and the discrete pressure domain). In this way the lubrication problem is solved in the half domain, reducing the evaluation cost severely.

$$\left.\frac{\partial \bar{p}}{\partial \bar{z}}\right|_{\bar{z}=1/2}=0, \qquad \frac{\bar{p}_{i,N_Z/2}-\bar{p}_{i,N_Z/2-1}}{\Delta \bar{z}}=0 \tag{5}$$

Last, the initial conditions for the dimensionless form of the problem are defined in Eq. (6) (in the continuous and the discrete pressure domain).

$$\bar{p}\left(\tau=0,\theta,\bar{z}\right)=1,\ \overset{\langle t_0\rangle}{\bar{p}}_{i,j}=1 \text{ and } \bar{q}\left(\tau=0,\theta\right)=0,\quad \overset{\langle t_0\rangle}{\bar{q}}_{i}=0 \tag{6}$$

After evaluating gas pressure $\bar{p}$ (as $\bar{p}_{i,j}$), the nonlinear gas forces are determined in Eq. (7), where $\Delta\bar{x}=2\pi/N_X$ and $\Delta\bar{z}=1/N_Z$.

$$\bar{F}_{B,X}=-\int_0^{2\pi}\int_0^1\left(\bar{p}-1\right)\cos\theta d\bar{z}d\theta=-\sum_{i=2}^{N_X}\sum_{j=2}^{N_Z}\left(\left(\bar{p}_{i,j}-1\right)\cos\theta_i\Delta\bar{x}\Delta\bar{z}\right) \tag{7a}$$

$$\bar{F}_{B,Y}=-\int_0^{2\pi}\int_0^1\left(\bar{p}-1\right)\sin\theta d\bar{z}d\theta=-\sum_{i=2}^{N_X}\sum_{j=2}^{N_Z}\left(\left(\bar{p}_{i,j}-1\right)\sin\theta_i\Delta\bar{x}\Delta\bar{z}\right) \tag{7b}$$

In this way the aerodynamic problem renders $N_X\cdot N_Z$ ODEs of 1st order with respect to the time derivative of the point pressure in Eq. (8)

$$\dot{\bar{\mathbf{p}}}=\left\{\dot{\bar{p}}_{i,j}\right\}=\mathbf{f}_B\left(\bar{\mathbf{p}},\bar{\mathbf{x}},\dot{\bar{\mathbf{x}}},\bar{\mathbf{q}},\dot{\bar{\mathbf{q}}}\right) \tag{8}$$

The vectors $\bar{\mathbf{x}}$ and $\bar{\mathbf{q}}$ may be perceived as $\bar{\mathbf{x}}=\left\{x_j \quad y_j \quad x_d \quad y_d\right\}^{\mathrm{T}}$ representing the journal motion (coupled to the disc motion through the rotor's equations of motion) and $\bar{\mathbf{q}}=\left\{\bar{q}_1 \quad \bar{q}_1 \quad \dots \quad \bar{q}_{N_X}\right\}^{\mathrm{T}}$ representing the foil motion (coupled to the journal motion through the Reynolds equation due to the gas film thickness function).

It is important to mention that it is quite common that sub-ambient pressure arises in GFBs. The sub-ambient pressure can cause the top foil to separate from the bumps into a position in which the pressure on both sides of the pad is equalized. Heshmat et al. [1] introduced a set of boundary conditions accounting for this separation effect. More specifically, a simple Gümbel boundary condition is imposed, meaning that sub-ambient pressures are discarded when integrating the pressure in Eq. (7) to obtain the bearing force components $\bar{F}_{B,X}$, $\bar{F}_{B,Y}$ essentially leaving the sub-ambient regions ineffective. In terms of numerical calculations, the assumption made by Heshmat [1] can be simply explained as following: in case fluid pressure p is lower than the ambient p_0, then the former should be considered equal to p_0 and the foil deformation at these points will be zero $\left(\bar{q}_i=0 \text{ for } \bar{p}_i<1\right)$.

The simplified model for the bump foil structure is depicted at Fig. 2b. The structure consists of N_X-2 linear massless elements of stiffness $\bar{k}_f$ (compliance $\bar{a}_f=1/\bar{k}_f$) and damping $\bar{c}_f$. The springs and dampers mount the corresponding N_X-1 top foil stripes of area $\Delta x\cdot L_b$ (or dimensionless area $\Delta\bar{x}\cdot 1$), see Fig. 3b. The top foil of the bearing is not covering a complete cylinder; a single gap can be found at $\theta=\theta_0$, see Fig. 2a, where the top foil is clamped to the bearing housing. Therefore, the moving top foil stripes are N_X-1, see Fig. 3b. The top foil stripes are assumed to remain parallel to the bearing longitudinal axis during their lateral motion, therefore no axial coordinate is required for the top foil motion. The geometry of the foil structure and its properties, shown in Figs. 2a and 3b, render the dimensionless compliance $\bar{\alpha}_f=2p_0\left(l_0/t_b\right)^3\left(1-v^2\right)s_0/\left(c_rE\right)$ [14]. The motion of each of the top foil stripe is excited by the mean gas pressure $\bar{p}_{m,i}$ acting on the top of it, creating the gas force $\bar{F}_B\left(i\right)$, see Figs. 2b and 3b. The mean gas pressure $\bar{p}_{m,i}$ is defined in Eq. (9) (in the continuous and discrete pressure domain respectively), for dimensional and dimensionless form.

$$p_m\left(\theta\right)=\frac{1}{L_b}\int_0^{L_b}p\left(\theta\right)dz,\quad p_{m,i}=\frac{1}{L_b}\sum_{j=2}^{N_Z}\left(p_{i,j}\Delta z\right),\qquad \bar{p}_{m,i}=\frac{1}{1}\sum_{j=2}^{N_Z}\left(\bar{p}_{i,j}\Delta\bar{z}\right)=\frac{1}{N_Z}\sum_{j=2}^{N_Z}\left(\bar{p}_{i,j}\right) \tag{9}$$

The foil stiffness and damping coefficient are given as $\bar{k}_f=1/\bar{\alpha}_f$ and $\bar{c}_f=\eta\bar{k}_f$ for foil motion synchronous to the excitation. The N_X-1 ODEs that describe the radial displacement $\bar{q}_i$ of the stripe i are defined in Eq. (10).

$$\bar{c}_f\dot{\bar{q}}_i+\bar{k}_f\bar{q}_i=\bar{p}_{m,i},\qquad i=2,3,\dots,N_X \tag{10}$$

The ODEs in Eq. (10) may be written as in Eq. (11) to be used in continue.

$$\dot{\bar{\mathbf{q}}}=\left\{\dot{\bar{q}}_i\right\}=\mathbf{f}_F\left(\bar{\mathbf{q}},\bar{\mathbf{p}},\bar{\mathbf{x}},\dot{\bar{\mathbf{x}}}\right) \tag{11}$$

Analytical model of the flexible rotor

The equations of motion for the Jeffcott rotor shown in Fig. 1 are defined in Eq. (12) for the journal and the disc, in the two main directions, horizontal and vertical.

$$\ddot{\bar{x}}_j = \frac{m_d}{2m_j}\bar{k}_s\left(\bar{x}_d - \bar{x}_j\right) + \xi \cdot \bar{F}_{B,X}\ , \qquad \ddot{\bar{y}}_j = \frac{m_d}{2m_j}\bar{k}_s\left(\bar{y}_d - \bar{y}_j\right) + \xi \cdot \bar{F}_{B,Y} - \sigma \tag{12a}$$

$$\ddot{\bar{x}}_d = -\bar{k}_s\left(\bar{x}_d - \bar{x}_j\right) + \bar{F}_{U,X}\ , \qquad \ddot{\bar{y}}_d = -\bar{k}_s\left(\bar{y}_d - \bar{y}_j\right) + \bar{F}_{U,Y} - \sigma \tag{12b}$$

The ODEs in Eq. (12) may be written in Eq. (13), in the state space representation, to be used in continue.

$$\dot{\bar{\mathbf{x}}} = \mathbf{f}_R\left(\bar{\mathbf{p}}, \bar{\mathbf{x}}, \dot{\bar{\mathbf{x}}}, \bar{\mathbf{q}}, \dot{\bar{\mathbf{q}}}\right) \tag{13}$$

In Eq. (12) $\bar{k}_s$ is the dimensionless shaft stiffness coefficient, and ξ , σ are dimensionless parameters defined in Eq. (14).

$$\xi = \frac{36\mu^2 LR^5}{m_j p_0 {c_r}^5}, \qquad \sigma = \frac{36\mu^2 R^2 g}{{p_0}^2 {c_r}^5} \tag{14}$$

In addition, in Eq. (12), $\bar{F}_{U,X}$ and $\bar{F}_{U,Y}$ are the dimensionless unbalance forces defined in Eq. (15a) for constant rotating speed $\bar{\Omega}$, and in Eq. (15b) for linearly varying rotating speed $\bar{\Omega} = \bar{a} \cdot \tau$ with constant acceleration $\bar{a}$.

$$\bar{F}_{U,X} = \varepsilon \cdot \bar{\Omega}^2 \cos\bar{\varphi}_r\ , \qquad \bar{F}_{U,Y} = \varepsilon \cdot \bar{\Omega}^2 \sin\bar{\varphi}_r\ , \qquad \bar{\varphi}_r = \bar{\Omega}\tau \tag{15a}$$

$$\bar{F}_{U,X} = \varepsilon\left(\bar{\Omega}^2 \cos\bar{\varphi}_r + \bar{a}\sin\bar{\varphi}_r\right), \qquad \bar{F}_{U,Y} = \varepsilon\left(\bar{\Omega}^2 \sin\bar{\varphi}_r - \bar{a}\cos\bar{\varphi}_r\right), \qquad \bar{\varphi}_r = \bar{a}\tau^2/2 \tag{15b}$$

Dimensionless unbalance eccentricity $\varepsilon = e_u / c_r$ follows in this paper the ISO unbalance grades (G-grades) for low, medium, and high unbalance as G1, G2.5 and G6.3 correspondingly. The unbalance located in the disc is of magnitude $u = \left(m_d + 2m_j\right)e_u$ at each case, and the corresponding eccentricity e_u is given by Eq. (16), where the service speed of the system is selected at $\Omega_r = 2500\,\text{rad/s}$.

$$e_u[\text{mm}] = \frac{G}{\Omega_r[\text{rad/s}]}, \qquad G = 1,\ 2.5,\ 6.3 \tag{16}$$

Composition and solution of the dynamic system

Eqs. (8), (11), and (13) compose a coupled ODE set which is composed by the discretized Reynolds equation in the $\mathbf{f}_B$ equations, the foil motion in $\mathbf{f}_F$ equations, and the rotor motion in $\mathbf{f}_R$ equations. The coupled nonlinear ODE set is defined in Eq. (17) expressing a non-autonomous dynamic system which will be studied with respect to the bifurcation parameter $\bar{\Omega}$. The ODE set is characterized as non-autonomous due to the explicit time presence in the equations of unbalance forces, see Eq. (15). The state vector $\bar{\mathbf{s}}$ and the respective functions $\mathbf{f}$ are defined in Eq. (18).

$$\dot{\bar{\mathbf{s}}} = \mathbf{f}\left(\bar{\mathbf{s}}, \bar{\Omega}, \tau\right) \tag{17}$$

$$\bar{\mathbf{s}} = \left\{\bar{\mathbf{p}} \quad \bar{\mathbf{q}} \quad \bar{\mathbf{x}}\right\}^{\mathrm{T}},\ \mathbf{f} = \left\{\mathbf{f}_B \quad \mathbf{f}_F \quad \mathbf{f}_R\right\}^{\mathrm{T}} \tag{18}$$

The total number of equations in Eq. (17) (size of vector function $\mathbf{f}$) is $N = \left(N_X \cdot N_Z\right) + \left(N_X - 1\right) + 8$ with the first term coming from the pressure equations, the second term coming from the foil equations, and the third term from the rotor equations in state space.

The ODE set in Eq. (17) renders the time response of the physical system when time integration is applied [32]. The system is numerically stiff and special algorithms are applied in time integration [32]. Furthermore, the Reynolds equation can be reduced in size applying an order reduction method [12], improving the computational cost. The time integration can handle both cases of unbalance equations, for constant rotating speed or for run-up, see Eq. (15).

An orthogonal collocation method [30] is applied for the computation of limit cycle motions produced by the ODE set in Eq. (17) at a constant $\bar{\Omega}$; Eqs. (15a) apply for unbalance forces at this case. Numerical continuation of limit cycles has been programmed by the authors according to pseudo arc length continuation method [29,33] with embedded collocation scheme [30]. The formulation of the method is defined also in Appendix A1. As the collocation method cannot handle non-autonomous ODE systems, Eq. (17) has to be converted to autonomous. This is achieved by coupling the ODE set of Eq. (17) with a two DoF oscillator, see Eq. (19), whose unique solution is a harmonic motion of frequency $\bar{\Omega}$, see Eq. (20) [30].

$$\dot{\bar{s}}_{N+1} = f_{N+1} = \bar{s}_{N+1} + \bar{\Omega} \cdot \bar{s}_{N+2} - \bar{s}_{N+1} \cdot \left(\bar{s}_{N+1}^2 + \bar{s}_{N+2}^2\right) \tag{19a}$$

$$\dot{\bar{s}}_{N+2} = f_{N+2} = -\bar{\Omega} \cdot \bar{s}_{N+1} + \bar{s}_{N+2} - \bar{s}_{N+2} \cdot \left(\bar{s}_{N+1}^2 + \bar{s}_{N+2}^2\right) \tag{19b}$$

$$\bar{s}_{N+1} = \cos\left(\bar{\Omega}\tau\right),\quad \bar{s}_{N+2} = \sin\left(\bar{\Omega}\tau\right) \tag{20}$$

The size of the final autonomous ODE set is $N+2$ and is defined in Eq. (21) with the unbalance forces to be defined at constant rotating speed, in Eq. (22).

$$\dot{\tilde{\bar{\mathbf{s}}}} = \tilde{\mathbf{f}}\left(\tilde{\bar{\mathbf{s}}}, \bar{\Omega}\right) \tag{21a}$$

$$\tilde{\bar{\mathbf{s}}} = \left\{\bar{\mathbf{s}}^{\mathrm{T}} \quad \bar{s}_{N+1} \quad \bar{s}_{N+2}\right\}^{\mathrm{T}},\qquad \tilde{\mathbf{f}} = \left\{\mathbf{f}^{\mathrm{T}} \quad f_{N+1} \quad f_{N+2}\right\}^{\mathrm{T}} \tag{21b}$$

$$\bar{F}_{U,X} = \varepsilon\cdot\bar{\Omega}^2\bar{s}_{N+1},\qquad \bar{F}_{U,Y} = \varepsilon\cdot\bar{\Omega}^2\bar{s}_{N+2} \tag{22}$$

Results and Discussion

The dynamic system defined in Eq. (19) in autonomous and in Eq. (20) in non-autonomous version is investigated on its potential to develop a variety of bifurcation sets with respect to the key design parameters, namely rotor stiffness $\bar{k}_s$, foil compliance $\bar{a}_f$, foil loss factor η, and unbalance magnitude u. In this paper, the key design parameters are defined within specific intervals, composing the case studies which are presented in continue. The design parameters follow a variation of "low", "reference", and "high". This is interpreted to the rotor stiffness values $\bar{k}_s = 0.3, 1, 3$ (flexible to rigid rotor), foil compliance values $\bar{a}_f = 0.01, 0.1, 1$ (stiff to flexible foil), foil loss factor $\eta = 0.005, 0.05, 0.5$ (low to high foil damping), and unbalance magnitude $u(G1), u(G2.5), u(G6.3)$ (low to high unbalance). A reference system is defined with the design parameters to be $\bar{k}_s = 1$, $\bar{a}_f = 0.1$, $\eta = 0.05$, and $u(G6.3)$.

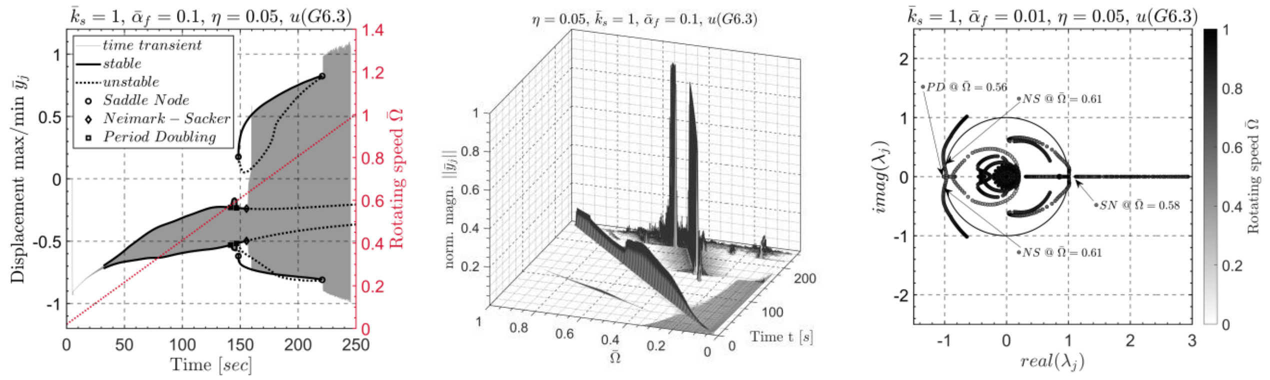

(a) (b) (c)

Figure 3: Reference system of $\bar{k}_s = 1$, $\bar{a}_f = 0.1$, $\eta = 0.05$, and $u(G6.3)$ a) Transient response and continuation of limit cycles during run-up b) STFT of the response time history c) Floquet multipliers of the corresponding limit cycles

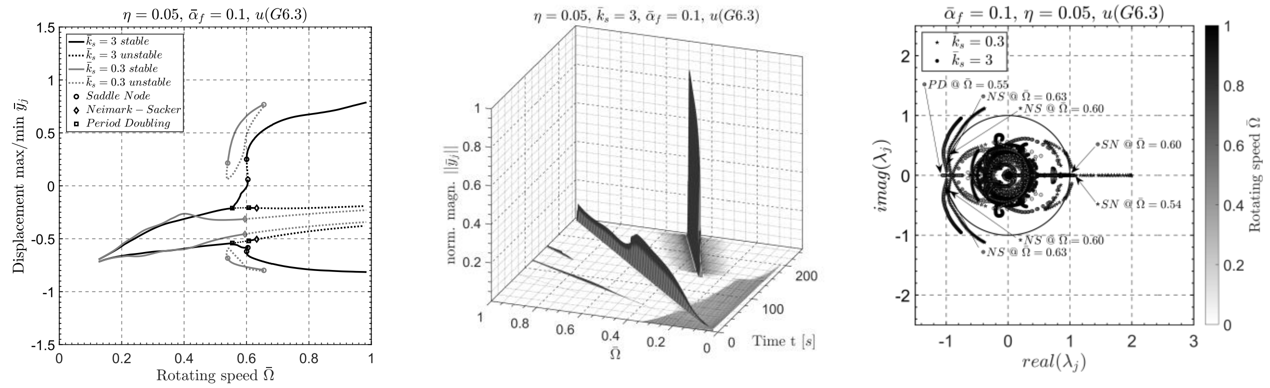

(a) (b) (c)

Figure 4: System of $\bar{k}_s^-, \bar{k}_s^+, \bar{a}_f = 0.1, \eta = 0.05, u = (G6.3)$ a) Continuation of limit cycles, b) STFT of the response time history $\bar{k}_s^+$, c) Floquet multipliers of the corresponding limit cycles.

In Fig. 3a the time history of the journal motion in the vertical plane is presented together with the maximum and minimum values of the limit cycle at each rotating speed. It has to be clarified that the rotating speed is retained constant when limit cycles are evaluated, and the unbalance forces are applied with different formulas in the ODE system in the transient run-up and in the ODE system for constant rotating speed. A reference bifurcation set is established in Fig. 3a with PD, SN, and NS bifurcations to be presented. The frequency content of the time history obtained during the run-up is depicted in Fig. 3b where time-frequency decomposition is applied. The Floquet multipliers in Fig. 3c provide information regarding the quality of bifurcations mentioned above. In Fig. 4 considers systems of different rotor stiffness, and two cases are presented in Fig. 4a for $\bar{k}_s^+ = 3$ and $\bar{k}_s^- = 0.3$. One may notice the difference compared to the reference case. Period doubling bifurcation is not noticed in this case.

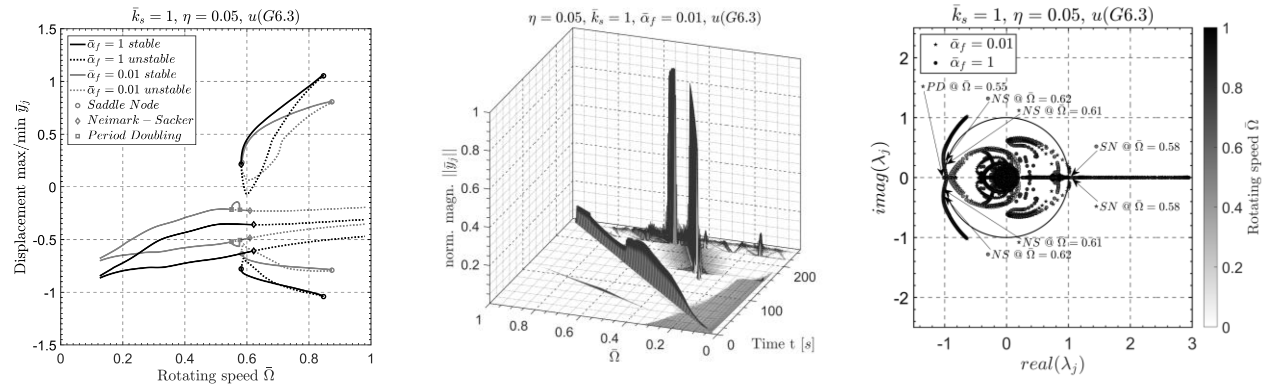

(a) (b) (c)

Figure 5: System of $\bar{k}_s = 1$, $\bar{a}_f^-, \bar{a}_f^+$, $\eta = 0.05$, $u = (G6.3)$. a) Continuation of limit cycles, b) STFT of the response time history for $\bar{a}_f^+$, c) Floquet multipliers of the corresponding limit cycles.

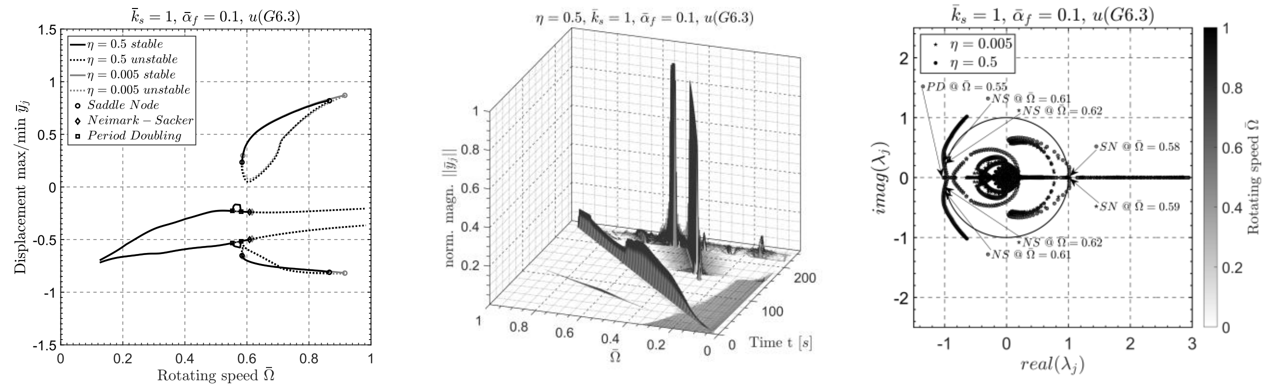

(a) (b) (c)

Figure 6: System of $\bar{k}_s = 1$, $\bar{a}_f = 0.1$, η^-, η^+, $u(G6.3)$. a) Continuation of limit cycles, b) STFT of the response time history for η^+, c) Floquet multipliers of the corresponding limit cycles for η^+.

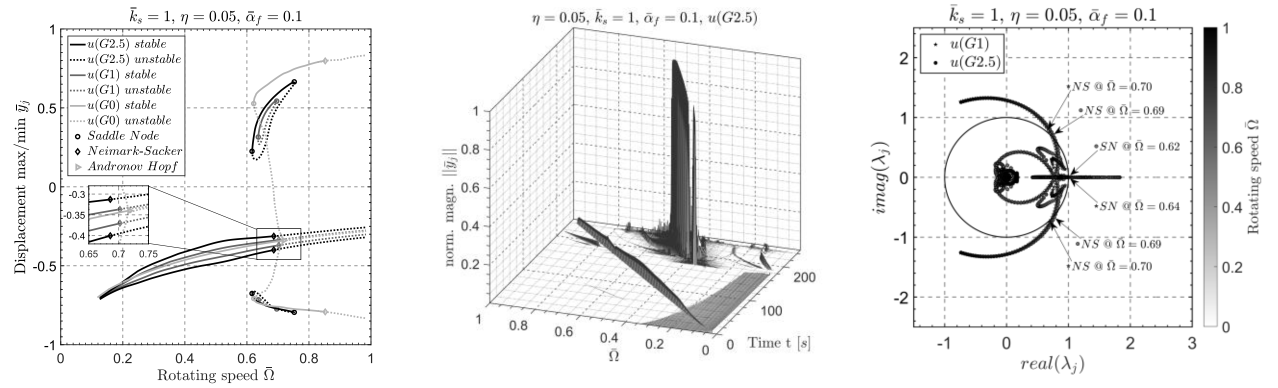

Figure 7: System of $\bar{k}_s = 1$, $\bar{a}_f = 0.1$, $\eta = 0.05$. a) Continuation of limit cycles, b) STFT of the response time history, c) trajectory, Poincare map, and FFT at $\bar{\Omega} = 0.97$, d) Floquet multipliers of the corresponding limit cycles.

In Fig. 5, systems of different foil compliance are considered, and two cases are presented in Fig. 5a, for $\bar{a}_f^+ = 1$ (flexible foil) and $\bar{a}_f^- = 0.01$ (rigid foil). One may notice the different bifurcation sets compared to the reference case, and the previous case. The type of bifurcations are same to this at the reference case, but the speed in which they appear is different.

In Fig. 6, systems of different foil damping are considered, and two cases are presented in Fig. 6a, for $\eta^{+} = 0.5$ (high foil damping) and $\eta^{-} = 0.005$ (low foil damping). The influence of foil damping in the bifurcation set is not severe, compared to the reference design (see Fig. 3).

In Fig. 7, systems of different unbalance are considered. It is worth noticing that the autonomous system of $u(G0)$ loses local stability of fixed point equilibria through an Andronov-Hopf bifurcation, at similar speed where the unbalanced systems lose local stability through NS bifurcations. Further to that, in the unbalanced systems, the higher the unbalance is, the lower the speed of NS bifurcations is. Stable limit cycles close to radial clearance occur with higher amplitude in the balanced system, than in the unbalanced systems. In the balanced system the limit cycles of amplitude close to radial clearance will lose stability through a NS bifurcation at high speeds.

Energy flow and optimization for bifurcation elimination

The work of the bearing forces is evaluated in Eq. (23a), the work of the bump foil forces is evaluated in Eq. (23b), and the work of unbalance forces in evaluated in Eq. (23c).

$$W_B = 2\sum_{i=1}^{N_t}\left(F_{B,X}(i)\cdot\delta x_j(i) + F_{B,Y}(i)\cdot\delta y_j(i)\right) = W_{cb} + \underbrace{W_{kb}}_{=0} \tag{23a}$$

$$W_f = 2\sum_{i=1}^{N_t}\left(\sum_{j=1}^{N_x} F_{f,j}(i)\cdot\delta q_j(i)\right) = W_{cf} + \underbrace{W_{kf}}_{=0}\,, \quad W_{fu} = \sum_{i=1}^{N_t}\left(F_{U,X}(i)\cdot\delta x_d(i) + F_{U,Y}(i)\cdot\delta y_d(i)\right) \tag{23b,c}$$

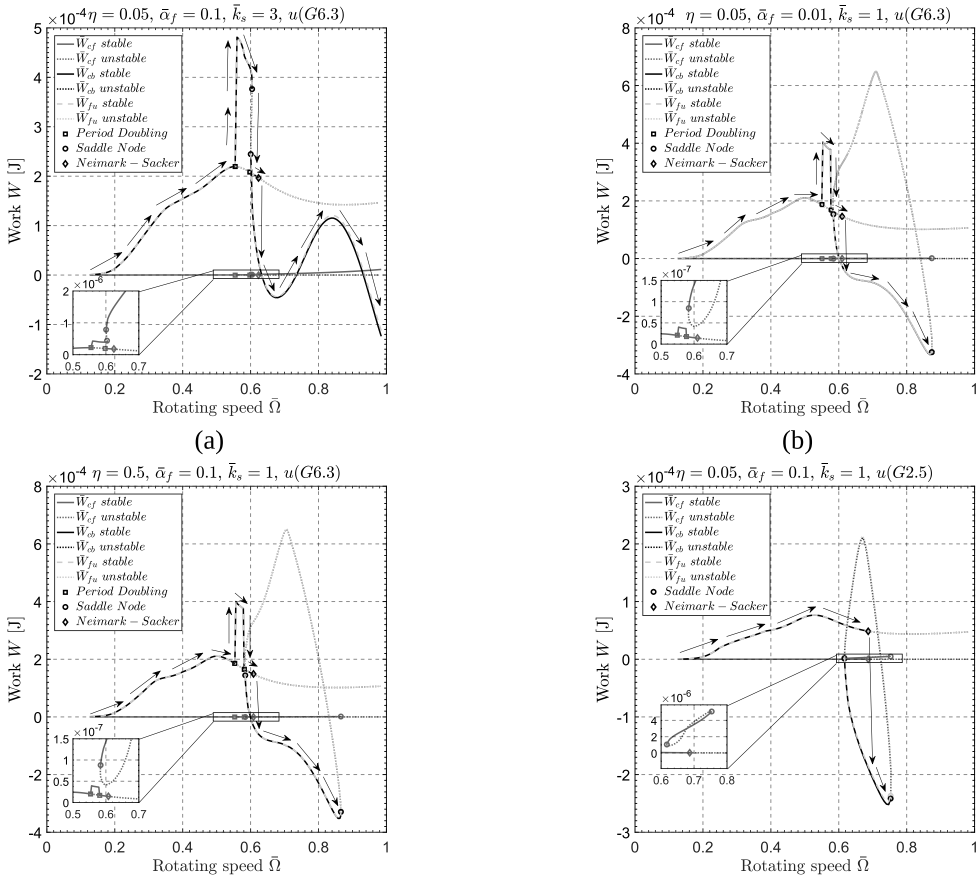

Figure 8: Evaluation of energy flow at the respective limit cycles for a) $\bar{k}_s = 3$, $\bar{a}_f = 0.1$, $\eta = 0.05$, $u(G6.3)$ b) $\bar{k}_s = 1$, $\bar{a}_f = 0.01$, $\eta = 0.05$, $u(G6.3)$, c) $\bar{k}_s = 1$, $\bar{a}_f = 0.1$, $\eta = 0.5$, $u(G6.3)$, and d) $\bar{k}_s = 1$, $\bar{a}_f = 0.1$, $\eta = 0.05$, $u(G2.5)$.

In Figs. 8a-d, both stable and unstable limit cycles are considered with the respective notation. At all cases, it is found that Neimark-Sacker bifurcations are triggered simultaneously to the reverse (from positive values to negative) of the dissipating work in the gas film W_{cb}, meaning that energy is not dissipated in the gas film (when $W_{cb} < 0$) and self-excitation takes place. The respective limit cycles for the cases in Fig. 8 can be found in the previous Section. In Figs. 8a-d, the arrows depict the path that would be followed during the run-up of the system (time integration).

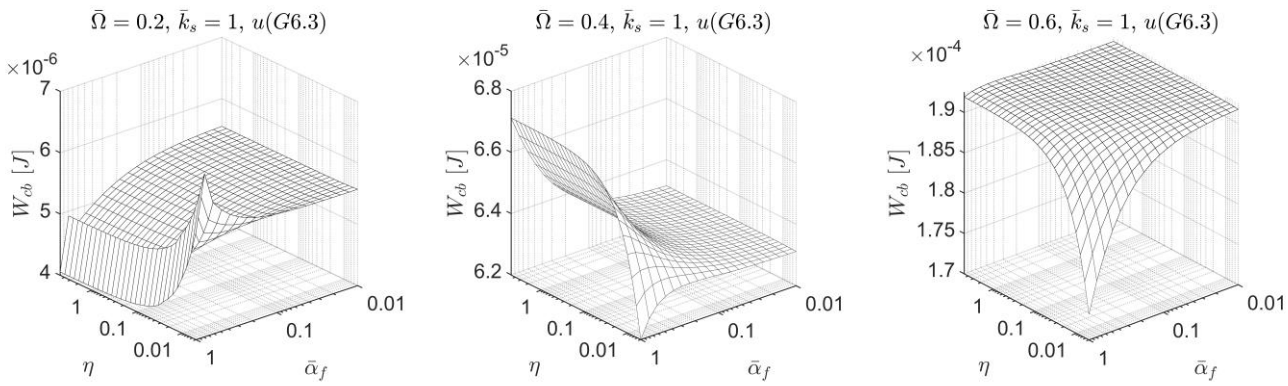

(a) (b) (c)

Figure 9: Dissipated energy in the gas film in one limit cycle for various values of foil compliance $\overline{a}_f$ and foil loss factor η, at a) $\overline{\Omega} = 0.2$, b) $\overline{\Omega} = 0.4$, c) $\overline{\Omega} = 0.6$

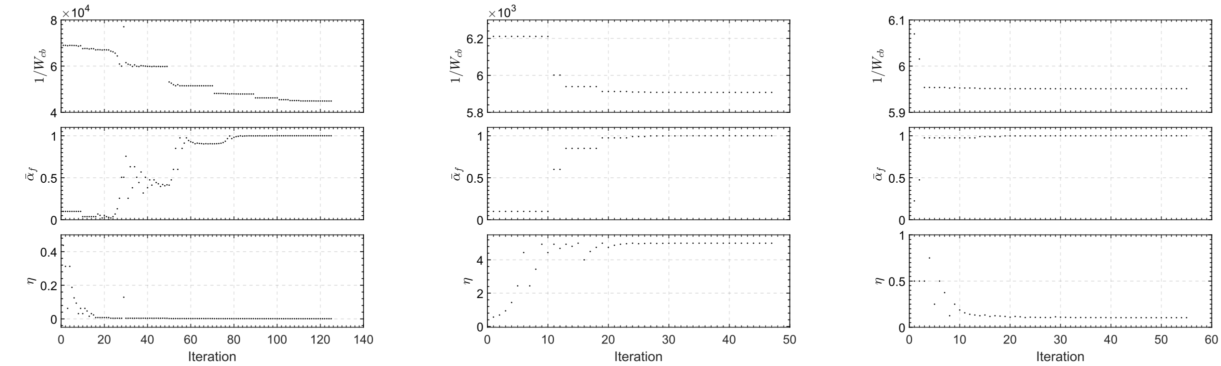

(a) (b) (c)

Figure 10: Optimization of the dissipated energy in the gas film of the reference system with $\overline{k}_s = 1$ and $u(G6.3)$ with respect to the foil compliance $\overline{a}_f$ and the foil loss factor η, at a) $\overline{\Omega} = 0.2$, b) $\overline{\Omega} = 0.4$, c) $\overline{\Omega} = 0.6$.

The optimization requires the minimization of an objective function OBJ, which is defined as the inverse of dissipated energy in the gas film, $OBJ = 1/W_{cb}$. Starting from random input values for foil compliance $\overline{a}_f$ and foil loss factor η, the optimization pattern renders after some iterations the values of $\overline{a}_f$ and η that maximize W_{cb} at every speed $\overline{\Omega}$. The limit cycle is plotted in Figs. 11 and 12 with the respective values $\overline{a}_f$ and η at each speed, for various design cases. Different rotor stiffness is considered in Fig. 11, and different unbalance magnitude applies in Fig. 12; the efficiency of the methodology to suppress bifurcations at a desired speed range is depicted. The operating speed range is limited by the limit values for the foil compliance $\overline{a}_f$ and the foil loss factor η, here defined as $0.01 \le \overline{a}_f \le 2$ and $0.0005 \le \eta \le 10$. These values may be considered differently according to the design limitations in each application of the rotating system. Considering the bifurcations sets evaluated in Section 3.2 for various designs, Figs. 15 and 16 depict elimination of bifurcations in approximately double speed range. It is also worth noticing that the bifurcation-free speed range is limited by a secondary Hopf (Neimark-Sacker) bifurcation at all cases of design.

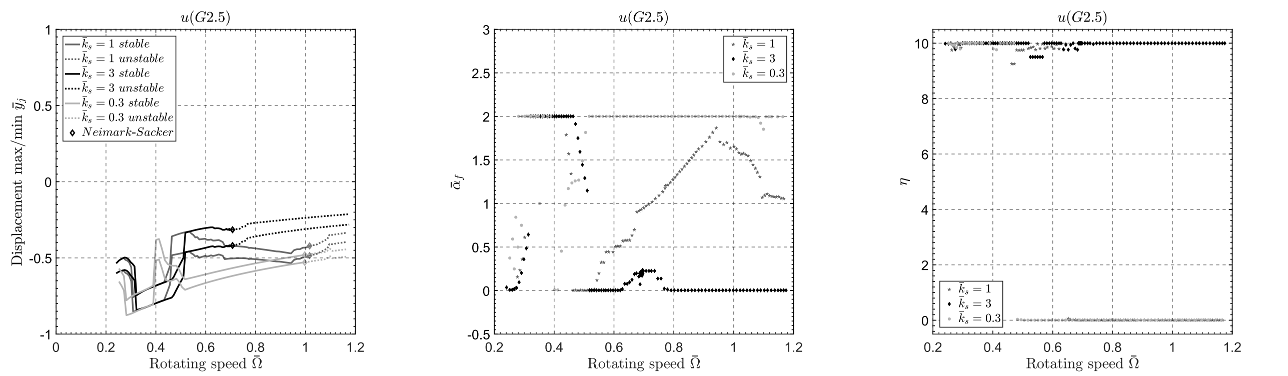

(a) (b) (c)

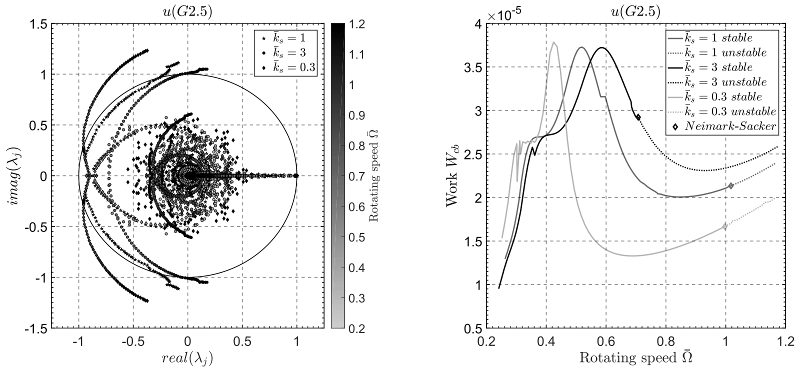

(d) (e)

Figure 11: Elimination of bifurcations at a speed range for the system of $u(G2.5)$ and $\bar{k}_s = 0.1$, $\bar{k}_s = 1$, $\bar{k}_s = 3$ a) journal motion limit cycles and corresponding values for b) compliance $\bar{a}_f$,c) loss factor η ,d) Floquet multipliers e) dissipating work in the gas film

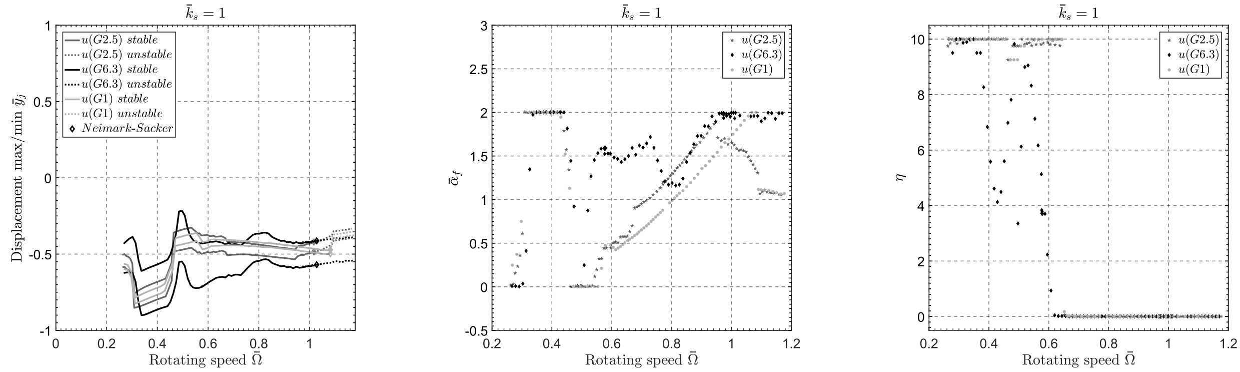

(a) (b) (c)

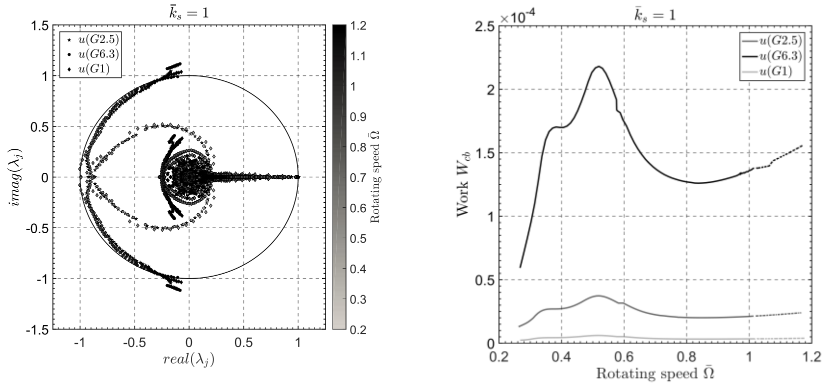

(d) (e)

Figure 12: Elimination of bifurcations at a speed range for the system of $\bar{k}_s = 1$ and $u(G1)$, $u(G2.5)$, $u(G6.3)$ a) journal motion limit cycles, and corresponding values for b) compliance $\bar{a}_f$ c) loss factor η ,d) Floquet multipliers e) dissipating work in the gas film

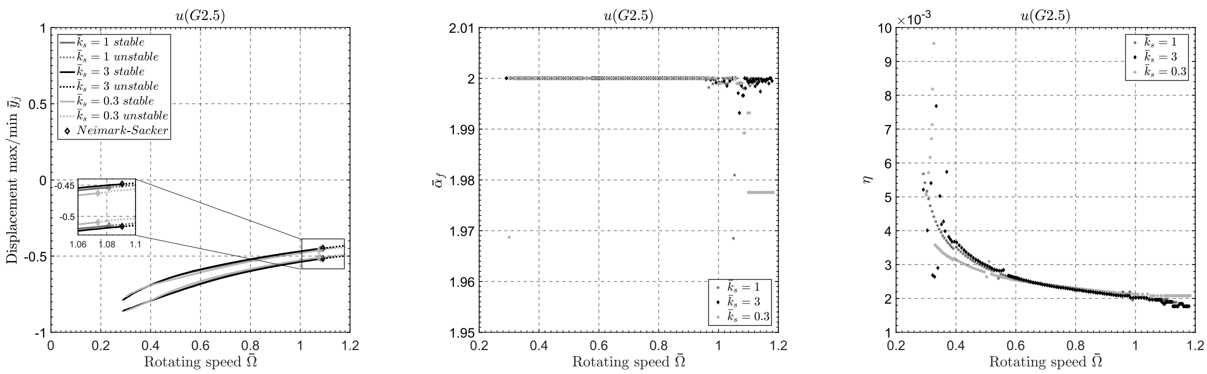

(a) (b) (c)

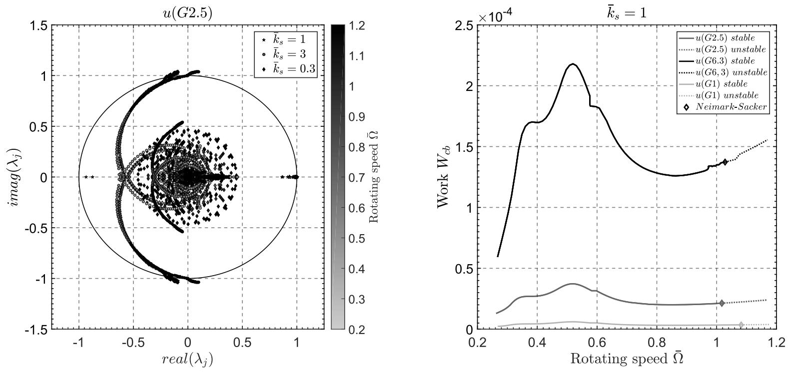

(d) (e)

Figure 13: Elimination of bifurcations at a speed range for the system of $u(G2.5)$ and $\bar{k}_s = 0.1$, $\bar{k}_s = 1$, $\bar{k}_s = 3$ a) journal motion limit cycles, and corresponding values for b) compliance $\bar{a}_f$,c) loss factor η d) Floquet multipliers e) dissipating work in the gas film

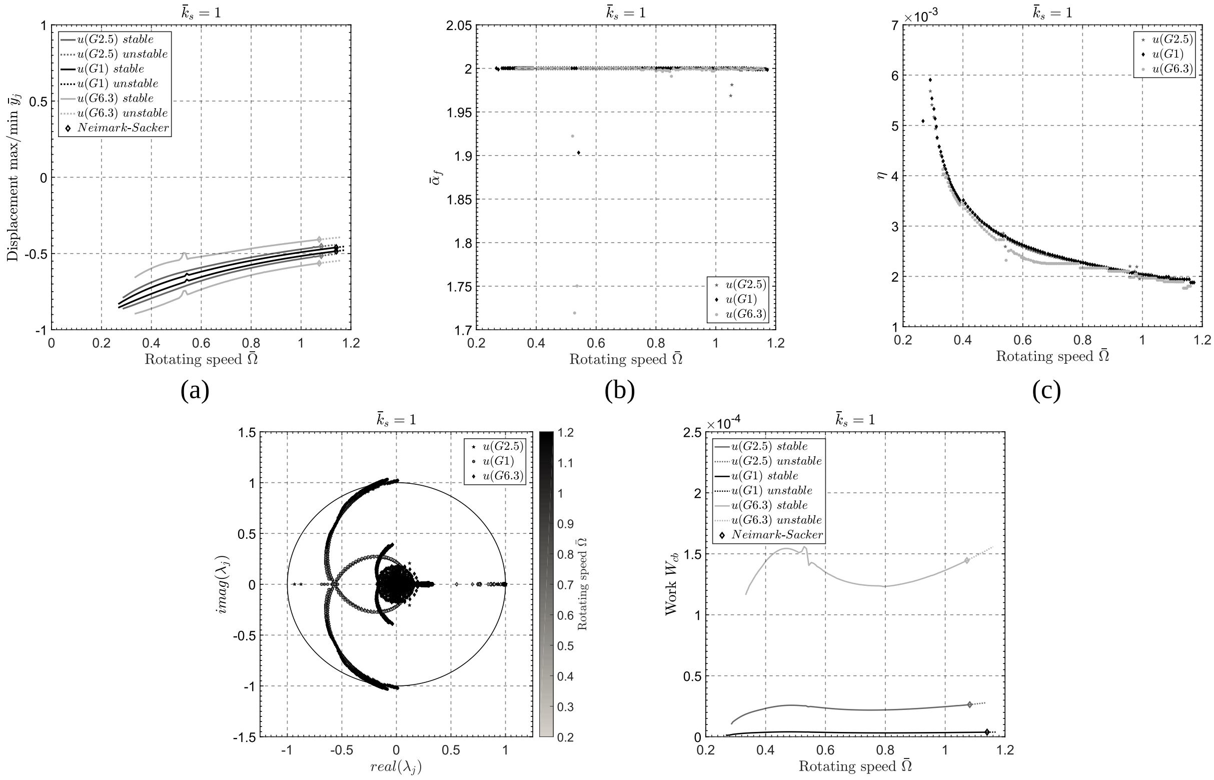

(a) (b) (c)

(d) (e)

Figure 14: Elimination of bifurcations at a speed range for the system of $\bar{k}_s = 1$ and $u(G1)$, $u(G2.5)$, $u(G6.3)$ a) journal motion limit cycles, corresponding values for b) compliance $\bar{a}_f$,c) loss factor η ,d) Floquet multipliers e) dissipating work in the gas film

An alternative objective function was investigated, in Figs. 13 and 14, on the potential to extend the operating speed range without bifurcation, at higher speeds. At each limit cycle $\overset{i}{\tilde{\mathbf{s}}}$, the highest magnitude of the Floquet multipliers was defined as objective function, $OBJ = \max\left(\left|\mu_j\right|\right)$, neglecting the one existing always at the unity circle, point $(+1,0)$. In this way, all Floquet multipliers are retained inside the unity circle, $\left|\mu_j\right| < 1$. The evaluation time of limit cycles was lower at this case, as the computation of dissipative work is not required. However, the applicability in a real system is questioned as it not of the authors' knowledge whether Floquet multipliers can be evaluated in real time. However, different index for stability is investigated by the authors though operational modal analysis.

Conclusions

The bifurcation set of a rotating shaft on gas foil bearings is presented in this paper for various design cases of rotor stiffness and gas bearing properties, in a certain range of rotating speed which acts as the bifurcation parameter. The periodic limit cycle motions are evaluated applying a pseudo arc length continuation method with embedded orthogonal collocation. The work of the non-conservative and nonlinear damping force of the gas film is evaluated at each limit cycle motion, even when unstable, as the collocation method allows for this possibility. The dissipative work of the gas film forces is found to be correlated to the self-exciting mechanism which triggers bifurcations of the solution branches for elastic unbalance response (stable motion). The loss of this local stability (through Neimark-Sacker bifurcation) occurs simultaneously with the reversal in the energy flow in the gas film, meaning that the dissipative work changes sign when the NS bifurcation takes place. At each limit cycle, an optimization pattern utilizing successive polls is applied to maximize the dissipated work in the gas film, defining the values for bump foil stiffness and damping, and thus avoid bifurcations according to the previous notation. The optimization pattern reveals that bifurcations are avoided when reducing the foil stiffness, doubling the operating speed range without bifurcations to take place. The procedure is repeated for several design scenarios of rotor stiffness and unbalance magnitude, and similar efficiency is noticed regarding bifurcation elimination. Research on design solutions to implement the change of foil damping and stiffness in a real system belongs to ongoing work.

Acknowledgments

The authors would like to thank *Alexander von Humboldt Foundation* for the funding of this work.

References

[1] Heshmat, H., Walowit, J., Pinkus, O.: Analysis of gas lubricated foil journal bearings. ASME J. Lubr. Technol 105(4), 647 (1983). https://doi.org/10.1115/1.3254697

[2] Agrawal, G.L.: Foil air/gas bearing technology-an overview, In: ASME 1997 International Gas Turbine and Aeroengine Congress and Exhibition, ASME Digital Collection, pp. 1–11(1997). https://doi.org/10.1115/97-GT-347

[3] DellaCorte, C.: Oil-Free shaft support system rotordynamics: Past, present and future challenges and opportunities. Mech. Syst. Signal Process. 29, 67–76 (2012). https://doi.org/10.1016/j.ymssp.2011.07.024

[4] Samanta, P., Murmu, N., Khonsari, M: The evolution of foil bearing technology. Trib. Int. 135, 305–323 https://doi.org/10.1016/j.triboint.2019.03.021

[5] Howard, S. A.; Bruckner, R. J.; DellaCorte, C.: Radil, K. C. Gas foil bearing technology advancements for closed Brayton cycle turbines. Tech. Rep. NASA TM-214470, National Aeronautics and Space Administration, United States of America (2007). https://doi.org/10.1063/1.2437506

[6] Howard, S. A.: Rotordynamics and design methods of an oil-free turbocharger. Tech. Rep. NASA CR-208689, National Aeronautics and Space Administration, United States of America (1999). https://doi.org/10.1080/10402009908982205

[7] Howard, S. A.; Bruckner, R. J.; Radil, K. C. Advancements toward oil-free rotorcraft propulsion. Tech. Rep. NASA TM-216094, US (2010)

[8] Vleugels, P., Waumans, T., Peirs, J., Al-Bender, F., Reynaerts, D.: High-speed bearings for micro gas turbines: Stability analysis of foil bearings. J. Micromech. Microeng. 16(9), S282 (2006). https://doi.org/10.1088/0960-1317/16/9/S16

[9] Peng, J.P., Carpino, M.: Calculation of stiffness and damping coefficients for elastically supported gas foil bearings. J. Tribol. 115(1), 20–27 (1993). https://doi.org/10.1115/1. 2920982

[10] San Andrés, L., Kim, T.H.: Forced nonlinear response of gas foil bearing supported rotors. Tribol. Int. 41(8), 704– 715 (2008). https://doi.org/10.1016/j.triboint.2007.12.009

[11] Leister, T., Baum, C., Seemann, W. Computational Analysis of Foil Air Journal Bearings Using a Runtime-Efficient Segmented Foil Model. ASME Journal of Fluids Engineering. 140(2) 021115 (2018). https://doi.org/10.1115/1.4037985

[12] Baum, C., Hetzler, H., Schröders, S., Leister, T., Seemann, W. A computationally efficient nonlinear foil air bearing model for fully coupled, transient rotor dynamic investigations. Tribol. Int. 153, 106434 (2020). https://doi.org/10.1016/j.triboint.2020.106434

[13] Pham, H., Bonello, P.: Efficient techniques for the computation of the nonlinear dynamics of a foil-air bearing rotor system, In: ASME Turbo Expo 2013: Turbine Technical Conference and Exposition, ASME Digital Collection, V07BT30A011 (2013). https://doi.org/10.1115/GT2013-94389

[14] Bhore, S.P., Darpe, A.K.: Nonlinear dynamics of flexible rotor supported on the gas foil journal bearings. J. Sound Vib. 332(20), 5135–5150 (2013). https://doi.org/10.1016/j.jsv.2013.04.023

[15] Larsen, J.S., Santos, I.F.: On the nonlinear steady-state response of rigid rotors supported by air foil bearings-theory and experiments. J. Sound Vib. 346, 284–297 (2015). https://doi.org/10.1016/j.jsv.2015.02.017

[16] Larsen, J.S., Santos, I.F., von Osmanski, S.: Stability of rigid rotors supported by air foil bearings: Comparison of two fundamental approaches. J. Sound Vib. 381, 179–191 (2016). https://doi.org/10.1016/j.jsv.2016.06.022

[17] Leister, T., Baum, C., Seemann, W.: On the Importance of Frictional Energy Dissipation in the Prevention of Undesirable Self-Excited Vibrations in Gas Foil Bearing Rotor Systems. Technische Mechanik 37, 2-5, 280 – 290 (2017). https://doi.org/10.24352/UB.OVGU-2017-104

[18] Hoffmann, R., Pronobis, T., Liebich, R.: Non-linear stability analysis of a modified gas foil bearing structure, In: Proceedings of the 9th IFToMM International Conference on Rotor Dynamics, Springer, pp. 1259–1276 (2015). https://doi.org/10.1007/978-3-319-06590-8_103

[19] von Osmanski, S., Larsen, J.S., Santos, I.F.: Multi-domain stability and modal analysis applied to gas foil bearings: Three approaches. J. Sound Vib. 472, 115174 (2020). https://doi.org/10.1016/j.jsv.2020.115174

[20] Feng, K., Cao, Y., Yu, K., Guan, H., Wu, Y., Guo, Z.: Characterization of a controllable stiffness foil bearing with shape memory alloy springs. Tribology International 136, 360-371 (2019). https://doi.org/10.1016/j.triboint.2019.03.068

[21] Anastasopoulos, L., Chasalevris, A.: Bifurcations of Limit Cycles in Rotating Shafts Mounted On Partial Arc and Lemon Bore Journal Bearings in Elastic Pedestals. ASME Journal of Computational and Nonlinear Dynamics (2022). https://doi.org/10.1115/1.4053593

[22] Gavalas, I., Chasalevris, A.: Nonlinear Dynamics of Turbine generator Shaft Trains: Evaluation of Bifurcation Sets Applying Numerical Continuation. ASME Journal of Engineering for Gas Turbine and Power. Accepted for publication (2022)

[23] Leister, T.: Dynamics of Rotors on Refrigerant Lubricated Gas Foil Bearings, Ph.D. Thesis, Karlsruhe Institute of Technology, Germany (2021)

[24] Chasalevris, A.: Stability and Hopf bifurcations in rotor-bearing-foundation systems of turbines and generators. Tribology International 145, 106154 (2020). https://doi.org/10.1016/j.triboint.2019.106154

[25] Le Lez, S., Arghir, M., Frene, J.: A new bump-type foil bearing structure analytical model. Journal of Engineering for Gas Turbines and Power 129(4), 1047–1057 (2007). https://doi.org/10.1115/1.2747638

[26] Ku, C. P., Heshmat, H.: Compliant foil bearing structural stiffness analysis: Part I-Theoretical model including strip and variable bump foil geometry. Journal of Tribology 114(2), 394–400 (1992). https://doi.org/10.1115/1.2920898

[27] Peng, J.P., Carpino, M.: Finite element approach to the prediction of foil bearing rotor dynamic coefficients. Journal of Tribology 119(1), 85–90 (1997). https://doi.org/10.1115/1.2832484

[28] Chen, W.J.: Energy analysis to the design of rotor bearing systems. ASME J. Eng. Gas Turb. and Power. 119(2), 411–417 (1997). https://doi.org/10.1115/1.2815590

[29] Doedel, E.J., Keller, H.B., Kernevez, J.P.: Numerical analysis and control of bifurcation problems (II): Bifurcation in infinite dimensions. International Journal of Bifurcation and Chaos 1(3), 745-772 (1991). https://doi.org/10.1142/S0218127491000555

[30] Doedel, E.J.: Lecture Notes on Numerical Analysis of Nonlinear Equations, Department of Computer Science, Concordia University, Montreal

[31] Nayfeh, A.H., Balachandran, B.: Applied nonlinear dynamics. J. Wiley & Sons (1995). https://doi.org/10.1002/9783527617548

[32] Shampine, L.F., Reichelt, M.W.: The MATLAB ODE Suite. SIAM J. Sci. Comput. 18(1), 1–22 (1997). https://doi.org/10.1137/S1064827594276424

[33] Meijer, H., Dercole, F., Olderman, B.: Numerical bifurcation analysis. Encyclopedia of Complexity and Systems Science, R. A. Meyers Ed., Springer New York, 6329-6352 (2009). https://doi.org/10.1007/978-0-387-30440-3_373